Surface & Coatings Technology 328 (2017) 134–141

Contents lists available at ScienceDirect

Surface & Coatings Technology

journal homepage: www.elsevier.com/locate/surfcoat

Characterization of magnetron sputtered sub-stoichiometric $CrAlSiN_x$ and $CrAlSiO_yN_x$ coatings

A. Al-Rjoub [a,*], P. Costa [a], L. Rebouta [a], M.F. Cerqueira [a,b], P. Alpuim [a,b], N.P. Barradas [c], E. Alves [d]

[a] Centre of Physics, University of Minho, Campus de Azurém, 4800-058 Guimarães, Portugal
[b] INL-International Iberian Nanotechnology Laboratory, Av. Mestre José Veiga, 4715-330 Braga, Portugal
[c] Centro de Ciências e Tecnologias Nucleares, Instituto Superior Técnico, EN 10, km 139.7, 2695-066 Bobadela LRS, Portugal
[d] Instituto de Plasmas e Fusão Nuclear, Instituto Superior Técnico, EN 10, km 139.7, 2695-066 Bobadela LRS, Portugal

ARTICLE INFO

Article history:
Received 27 May 2017
Revised 25 July 2017
Accepted in revised form 15 August 2017
Available online 15 August 2017

Keywords:
$CrAlSiN_x$
$CrAlSiO_yN_x$
Optical properties
Hardness
Chemical structure

ABSTRACT

The influence of varying nitrogen and oxygen partial pressures on microstructure, mechanical and optical properties of magnetron sputtered $CrAlSiN_x$ and $CrAlSiO_yN_x$ coatings has been studied. The partial pressure of nitrogen reactive gas was varied from 0.037 Pa to 0.15 Pa for $CrAlSiN_x$ films, and the N_2/O_2 (85%:15%) partial pressure was varied from 0.046 Pa to 0.21 Pa for $CrAlSiO_yN_x$ layers. Transmittance and reflectance of samples were measured and were modeled to obtain the spectral optical constants, n and k. Chemical state, composition, morphology and microstructure of films were analyzed by XPS, RBS, XRD, Raman Spectroscopy and SEM. Films' hardness was evaluated using nanoindentation method. XRD results revealed that the two samples $CrAlSiN_x$ with $P_N = 0.15$ Pa and $CrAlSiO_yN_x$ with $P_{NO} = 0.21$ Pa are polycrystalline with cubic (fcc-B_1) structure. On contrary, all other films prepared with lower reactive gases partial pressures are amorphous. The chemical composition changed with the variation of reactive gases partial pressure, although the Cr: Al: Si composition ratio remained approximately constant, 1.25:1.5:1. All samples showed low hardness, mainly due to lower content of reactive gases and higher content of Si. However, the sample $CrAlSiN_x$ with $P_N = 0.15$ Pa has the highest value of 11.1 GPa. Optical constants are seen to be very sensitive to reactive gases partial pressure. The refractive index and extinction coefficient were lower for coatings with higher reactive gases partial pressure. These coatings are good candidates for designing selective solar absorber stacks for different applications.

1. Introduction

$CrAlSiN_x$ and $CrAlSiO_yN_x$ are examples of multi-elemental thin films [1]. Recently, enormous studies and technological efforts have been devoted to the research on those kinds of materials, due to their excellent properties and numerous industrial applications. Chromium nitrides, oxides and oxy-nitrides generally have high oxidation resistance [2–9], chemical and thermal stability at high temperature [10–15], good thermal diffusion barrier [16], good corrosion resistance [17] and high hardness [18–22]. The numerous applications are divided into two main groups. First one is the optical and electrical applications such as, optical detectors, sensors, optical filters, lenses, emitting diodes, on concentrating solar power (CSP) [23–28] and phase shifting masks [29,30]. The second group is for plastic metal molds, cutting and drilling tools [31,32], due to their high hardness and wear resistance. This paper is devoted to study the influence of varying nitrogen and oxygen partial pressures on microstructure, mechanical and optical properties of sputtered $CrAlSiN_x$ and $CrAlSiO_yN_x$ coatings in the sub-stoichiometric range, where the ratio (O + N) / (Cr + Al + Si) is lower than 1. In literature [33,34], it is found that hard nano-composite coatings based of nc-CrN/a-SiN_x are optically opaque. This would be enough for a coating with high solar absorption, but not sufficient to have a coating with low emissivity. On the other hand, adding aluminum to Cr-Si-N changes the grain size, the composition and the mechanical properties of those materials, and tend to be amorphous and more transparent. This leads to an improvement of oxidation resistance properties and opens the possibility to tune the optical properties. Moreover, Oxygen content in films affect the whole coating properties, as an example, if oxygen content in oxynitrides increase, then films will be more transparent with lower refractive index, because of losing of their metallic behavior. Also, hardness values of such coatings remain low (12–13 GPa) in the range of oxygen ratio [O]/[O + N] of 20%–50% in films as reported by Karimi et al. [1] [8]. So, adjusting oxygen and nitrogen contents enables to control the optical, chemical, mechanical and electrical properties of $CrAlSiN_x$ and $CrAlSiO_yN_x$ coatings within a wide range [1,8,35,36]. Despite there are a lot of studies about nitride and oxy-nitrides, only limited researches focus on sputtered $CrAlSiN_x$ and $CrAlSiO_yN_x$ coatings. However, for these coatings exist in the literature devoted to the microstructure or mechanical properties studies.

* Corresponding author.
E-mail address: id5811@alunos.uminho.pt (A. Al-Rjoub).

http://dx.doi.org/10.1016/j.surfcoat.2017.08.038
0257-8972/

The main objective of the present work is to understand the optical properties of these coatings as varying reactive gases pressure, such that it can be used in structural designs of solar selective absorber stacks for high temperature applications. In addition, to study the influence of varying nitrogen and oxygen partial pressures on microstructure, mechanical properties of the coatings.

2. Experimental

A series of thin individual layers of $CrAlSiN_x$ and $CrAlSiO_yN_x$ were deposited on glass substrates with different nitrogen and oxygen partial pressures as reactive gases, as shown in Table 1. These thin layers were used to track the influence of varying those partial pressures upon optical properties of sputtered $CrAlSiN_x$ and $CrAlSiO_yN_x$. For morphology, chemical composition, crystalline structure and mechanical properties studies, thicker samples were deposited on (100)-oriented silicon wafer (used for SEM, XRD, XPS and RBS analysis) and polished stainless-steel substrates (used for nanoindentation tests) with same parameters as thinner ones, as shown in Table 2. Silicon wafer and stainless-steel substrates were ultrasonically cleaned in acetone for 15 min. The depositions were performed at room temperature in a vacuum chamber which evacuated up to 2×10^{-4} Pa base pressure. A pulsed dc bias of −60 V (frequency 90 kHz) was applied to the substrate holder during all depositions. The deposition times were fixed as 1 min and 30 min for thin and thick layers, respectively. The target (Chromium-Aluminum, 70–30 at% with nine 1 cm diameter silicon discs, 99.9% purity) was sputter cleaned in Ar atmosphere for 3 min. An additional Ar ion etching step was implemented for 15 min to clean the substrates using a voltage of −500 V. The target current density was 6.2 mA/cm^2, and the argon flow was adjusted to reach a constant total pressure of 0.37 Pa.

The crystalline structure of the samples was analyzed by using X-ray diffraction employing a Bruker AXS Discover D8 operating with Cu Kα radiation. The measurements were performed at an incidence angle of $\alpha = 3°$. Scanning electron microscopy (SEM) was performed with a Nano SEM–FEI Nova 200(FEG/SEM) microscope. Energy dispersive X-ray spectroscopy (EDS) analyzes were performed with the electron beam of the SEM, with an energy of 10 keV (EDAX – Pegasus X4M system). Nanoindentation tests were performed by using nano/microindentation-Micro Materials equipment, that has: load range up to 500 mN, load resolution 50 nN, depth range 0–50 mm and contact force <5 mN. Nanoindentation tests were applied with maximum loads ranged between 6 and 8 mN. Then, hardness and elastic modulus data were obtained using the method proposed by Oliver and Pharr [37]. The measurements were repeated five times for each specimen. Raman scattering measurements were carried out on alpha300 R confocal Raman microscope (WITec) using a 532 nm Nd: YAG laser for excitation. The system was operated with an output laser power of 2.5 mW. The laser beam was focused on the sample by a ×50 lens (Zeiss); and the spectra were collected with a 600 groove/mm grating using 5 acquisitions with a 2 s acquisition time. Rutherford back scattering (RBS) measurements were done at the CTN/IST Van de Graaff accelerator at the small chamber were three detectors are installed: standard at 140°, and two pin-diode detectors located symmetrical to each other, both at 165°. Spectra were collected for 2 MeV $^4He^+$, and 2.3 MeV $^1H^+$. Normal incidence was used in the experiments and the obtained data were analyzed with the IBA Data Furnace NDF [38]. Chemical composition and chemical bonding were evaluated using X-ray photoelectron spectroscopy (XPS). The measurements were performed using a Kratos AXIS Ultra HSA X-ray photoelectron spectroscopy (XPS) system, with an AlKα (1486.7 eV) X-ray source and with 40 eV pass energy. Binding energy was referenced to the C 1 s peak position at 285.0 eV to avoid the influence of the electro-static charging effects of samples. Data analysis and peaks fitting of the XPS spectra were performed by using the CasaXPS software with Shirley background and GL(30)line shape[1] [39].

Optical measurements, in transmittance and reflectance modes, were performed in the wavelength range of 250–2500 nm, using a Shimadzu PC3101 UV–VIS–NIR scanning spectrophotometer. The reflectance measurements were performed at an incidence angle of 8° using an integrating sphere attachment and an Al mirror as a reference. The reflectance data were corrected according to the Al-reference reflectance curve.

Table 1
Oxygen and nitrogen partial pressures of reactive gases in deposition for thin single layers (<100 nm) used to track the optical properties of sputtered $CrAlSiN_x$ and $CrAlSiO_yN_x$. Deposition rates were calculated using SCOUT software.

Nitride layer	N_2 partial pressure (Pa)[a]	Deposition rate [nm/min]	Oxynitride Layer	N_2/O_2 (85:15) partial pressure (Pa)[a]	Deposition rate [nm/min]
1	0.037	47.0	1	0.046	45.9
2	0.051	37.6	2	0.064	42.1
3	0.056	35.9	3	0.068	40.6
4	0.060	33.7	4	0.075	38.8
5	0.071	31.0	5	0.092	28.7
6	0.15	17.3	6	0.21	18.6

[a] P_{NO} will be used in instead of N_2/O_2 (85:15) Partial pressure and P_N instead of N_2 Partial pressure.

3. Results and discussion

3.1. Optical properties

Fig. 1 shows the transmittance (T) and reflectance (R) spectra of $CrAlSiN_x$ deposited at different N_2 partial pressure, from 0.037 Pa to 0.15 Pa and of $CrAlSiO_yN_x$ films deposited at different N_2/O_2 partial pressure, from 0.046 Pa to 0.21 Pa.

The results presented in Fig. 1a show that the $CrAlSiN_x$ and $CrAlSiO_yN_x$ layers become more transparent and lose their metallic behavior as the nitrogen and oxygen partial pressures increase. This is mainly due the presence of to Al and Si nitrides and oxides, which are transparent. In accordance with this, the reflectance in the same wavelength range decreases with increasing nitrogen and oxygen partial pressures. The optical constants, refractive index (n) and extinction coefficient (k), and layers thicknesses were determined from (T) and (R) curves [40] by using optical simulation program SCOUT [41]. These thicknesses were used to calculate the deposition rates shown in Table 1, which are slightly lower than those calculated by using the thicknesses of thicker samples, measured by SEM that shown in Table 2. Fig. 2 shows the optical constants, refractive index (n) and extinction coefficient (k), as a function of wavelength in the range of 250–2500 nm, which were obtained from the modeling of experimental T and R spectra. The results shown in the figure indicate a general behavior of n and k with a decrease as increasing the gases partial pressures for both nitride and oxynitride layers. Increasing oxygen and nitrogen amount in films caused an increment in its fraction bonds with other metals in films. Moreover, it is seen that the refractive indices for the $CrAlSiN_x$ layers increase in the wavelength range 250–1000 nm, which make these layers appropriate materials for selective absorption of solar radiation and other optical applications. The refractive index of $CrAlSiO_yN_x$ layers also shows a similar behavior with wavelength, but for higher gases partial pressures it becomes almost constant. The oxygen induces a decrease in both, the refractive index and extinction coefficient, for values that is not possible to get with nitride. For example, the minimum refractive index for nitrides is higher than 2.5, while with oxynitrides it is possible to tune it down to 1.6. A similar effect can be seen for the extinction coefficient, where in oxynitrides can be tuned down to zero, while in nitrides is always higher than 0.2. This behavior is also related with the Cr amount, which cannot be below a

[1] GL (p): Gaussian/Lorentzian product formula where the mixing is determined by m = p/100, GL (100) is a pure Lorentzian while GL (0) is pure Gaussian.

Table 2
Oxygen and nitrogen partial pressures as reactive gases in deposition individual thick layers (> 1 μm) used for morphology, chemical composition and microstructure of $CrAlSiN_x$ and $CrAlSiO_yN_x$. Deposition rates were calculated using thicknesses measured by SEM.

Nitride layer	N_2 partial pressure (Pa)	Thickness SEM (μm)	Deposition rate [nm/min]	Oxynitride layer	N_2/O_2 (85:15) partial pressure (Pa)	Thickness SEM (μm)	Deposition rate [nm/min]
1	0.033	1.46	48.8	1	0.046	1.29	43.0
2	0.040	1.36	45.2	2	0.053	1.26	42.0
3	0.051	1.26	42.1	3	0.064	1.17	39.0
4	0.056	1.25	41.8	4	0.075	1.08	36.0
5	0.060	1.19	39.6	5	0.092	1.06	35.5
6	0.15	0.52	17.3	6	0.21	0.56	18.7

certain value in order to have the adequate extinction coefficient for the high absorption layer.

As represented in Tables 1 and 2, the deposition rate decreases with increasing oxygen and nitrogen partial pressures. This is due to the formation of nitrides and oxynitrides bonds with the target surface elements during the film growth (known as target poisoning) [42], resulting in a reduction of sputtered materials and consequently of the deposition rate.

3.2. Chemical composition

As far as Rutherford backscattering spectrometry (RBS) is suitable for analysis of compositional depth profiles of amorphous structures, it was used in this work to analyze the samples' elemental compositions. Fig. 3 shows three typical RBS spectra, namely one of a nitride layer (Fig. 3a) and two of oxynitrides layers (Fig. 3b). Since the signals from the different elements overlap, the composition has to be determined from the front edges of the elements, which are indicated in the figure. The relative heights of those front edges are correlated with the relative concentrations of the different elements, and by the analysis of all samples (not shown) it was verified that the (Al + Si) / Cr composition ratio is about 2 and similar for different samples, as presented in Fig. 4 for all the nitride and oxynitride samples. With the used conditions, RBS technique is not adequate to have an enough separation between Al and Si front edges. So, EDS technique was used to measure the Al/Si ratio, which is in average 1.5. This means that the Cr:Al:Si ratio composition is 1.25:1.5:1. Fig. 4 also represents the chemical composition ratio (Cr + Al + Si) / (N + O) as a function of the reactive gases partial pressure, P_N in $CrAlSiN_x$ samples and P_{ON} in $CrAlSiOyN_x$ samples. In both cases, that compositional ratio decreases with increasing reactive gases pressures, as expected, which means, an increase of the nitrogen and oxygen contents. Moreover, a small amount of oxygen was detected in pure nitrides samples.

For more details about the chemical structure, three samples: (A) $CrAlSiN_x$ with $P_N = 0.056$ Pa, (B) $CrAlSiOyN_x$ with $P_{ON} = 0.046$ Pa and (C) $CrAlSiOyN_x$ with $P_{ON} = 0.075$ Pa have been chosen for XPS analysis. Fig. 5 shows the evaluated XPS spectra of Cr 2p, Al 2p, Si 2p, N 1 s and O 1 s core levels, while in Table 3 the Casa software fitting parameters and identification of core levels binding energies are represented. As shown in Fig. 5a, the XPS spectra of Cr $2p_{3/2}$ binding energy can be deconvoluted into three sub-peaks in the case of samples A and B. The respective energies of 574.1 eV, 574.8 eV and 577.4 eV correspond to metallic Cr, CrN and Cr_2O_3, respectively [7,43–47]. For higher partial pressure of P_{ON} as in sample C, the peaks corresponding to metallic Cr and CrN were not observed and a new peak centered at 576.1 eV appears, which may be an overlap between Cr-O and Cr_2N. Moreover, the Cr $2p_{3/2}$ doublet shifts towards higher binding energy with increasing oxygen content in the films, which indicates an increment of oxidized species in films [20].

For Al 2p spectra, the oxynitride samples revealed two peaks located at 74.5 and 75.4 eV, as shown in Fig. 5b, whereas for the nitrides another peak is seen, centered at 73.9 eV due to higher content of nitrogen in the film. The peaks at 74.5 eV and 75.4 eV are considered as $Al(OH)_3$ and Al_2O_3 compounds, respectively [48], and the third peak 73.9 eV is recognized as AlN [6,14,18,49].

Fig. 5c shows the Si 2p core level spectra, and it is seen that the peaks of samples A and B correspond to the contribution of three distinct components, while the peak of sample C only has two components. The peak centered at 103.0 eV in all three samples is recognized as silicon oxides in the form of Si(Al)-SiO_3 or SiO_4 bonds [48,50], considering a silicon-

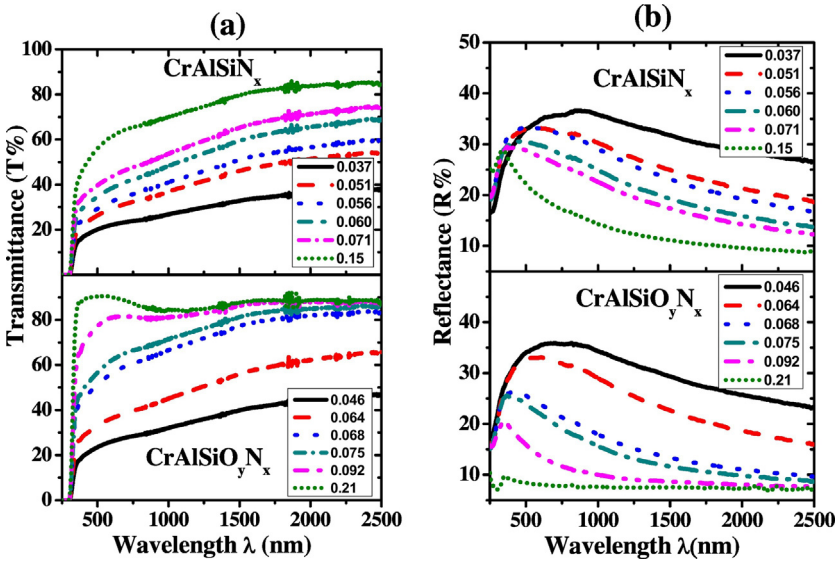

Fig. 1. Transmittance (a) and Reflectance (b) of $CrAlSiN_x$ and $CrAlSiO_yN_x$ as a function of oxygen and nitrogen partial pressures.

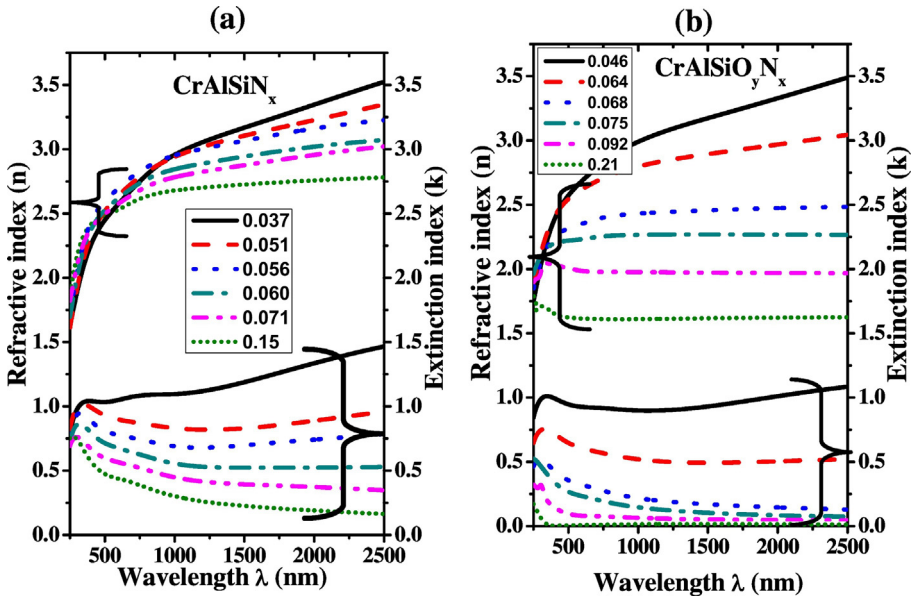

Fig. 2. Refractive index (n) and extinction coefficient (k) as a function of wavelength of: (a) $CrAlSiN_x$, prepared with increasing nitrogen partial pressures. (b) $CrAlSiO_yN_x$ as a function of wavelength, prepared with increasing nitrogen and oxygen partial pressures.

centered tetrahedrons, in which silicon, oxygen and nitrogen atoms are bonded in the form of any of the four tetrahedral sites of $Si–Si_{4-(m+n)}O_mN_n$ (where $m + n \leq 4$; $m,n = 0–4$) and the chemical shift of Si 2p level for each of the four tetrahedral is proportional to the partial charge on the Si atom [51]. The 99.3 eV component that appears in sample A and B could be Si-Si(Al) [14]. The last peak of sample A located at 101.5 eV is recognized as Si_3N_4 bond [2,7,14,19], and the peak at 102.3 in sample B and C is related to the formation of silicon oxynitrides $Si-N_3O$ or $Si(Al)-SiO_2N$ bonds [20,48].

As shown in (Fig. 5d), the XPS spectra of N 1s core level can be deconvoluted into five peaks. The peaks at energies 397.3, 398.2 and 399.9 eV can be associated to Si_3N_4 [19,46], chromium oxynitride [52] and $Si(Al)—O_2N_2$ [46]bonds, respectively. The fourth chemical component that appears only in sample A is located at 396.7 eV, and it describes Al—N bonds [19,48,52–53]. The peak in sample B located at 401.1 eV is related to CH═N—CH surface contamination.

As shown in Fig. 5e, the O1s spectra were not fitted into its components' peaks because it is difficult to identify their bonding energy. However, it should contain several peaks that can describe the chemical composition of samples. It is worthy to mention that the position of the oxygen peak shifts to higher energies with increasing the percentage of oxygen in films due to formation of oxides and oxynitrides, in accordance with what was reported in the literature [20].

From corresponding core-level intensities and tabulated atomic sensitivity factors, the relative atomic concentrations were calculated. Due to surface contamination, the oxygen is significantly larger than those measures by RBS and EDS. Additionally, the average (Al + Si) / Cr composition ratio for these 3 samples is now 4.1, two times higher than the bulk composition ratio obtained by RBS and EDS, and the Al/Si ratio also revealed an increase (1.9 instead of 1.5, in average). Considering that XPS measures the elements and the quantity of those elements that are present within the top 1–10 nm of the sample surface, this means that surface contamination led to an Al surface enrichment and a significant Cr depletion.

3.3. Phase content and crystalline structure

Thick layers of $CrAlSiN_x$ and $CrAlSiOyN_x$ deposited on silicon wafer substrates were used for X-ray diffraction, the X-ray diffractograms are shown in Fig. 6. In the diffractograms of $CrAlSiN_x$ and $CrAlSiOyN_x$ films in the ranges of $P_N = 0.037–0.071$ Pa and $P_{NO} = 0.046–0.091$ Pa, respectively, no strong peaks were observed, which means they are XRD amorphous. For higher nitrogen and oxygen partial pressures,

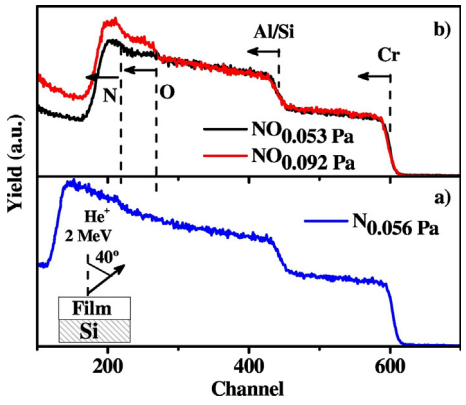

Fig. 3. RBS spectra of: (a) nitride layer and (b) two different oxynitride layers.

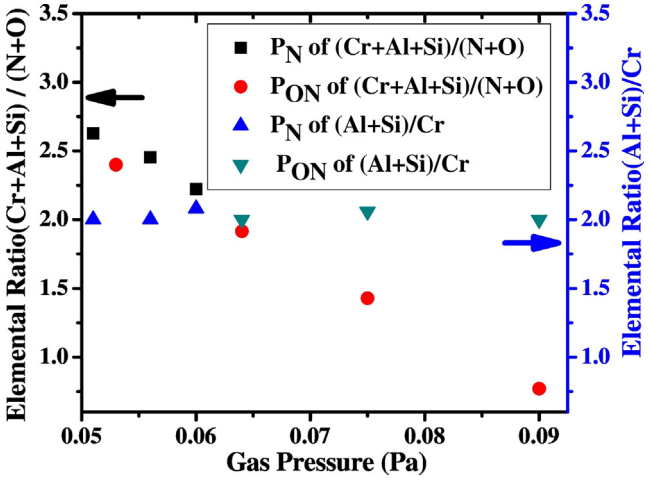

Fig. 4. Elemental composition ratios (Cr + Al + Si) / (N + O) and (Si + Al) / Cr in films as a function of P_N for $CrAlSiN_x$ and P_{ON} for $CrAlSiO_yN_x$ films as evaluated by (RBS).

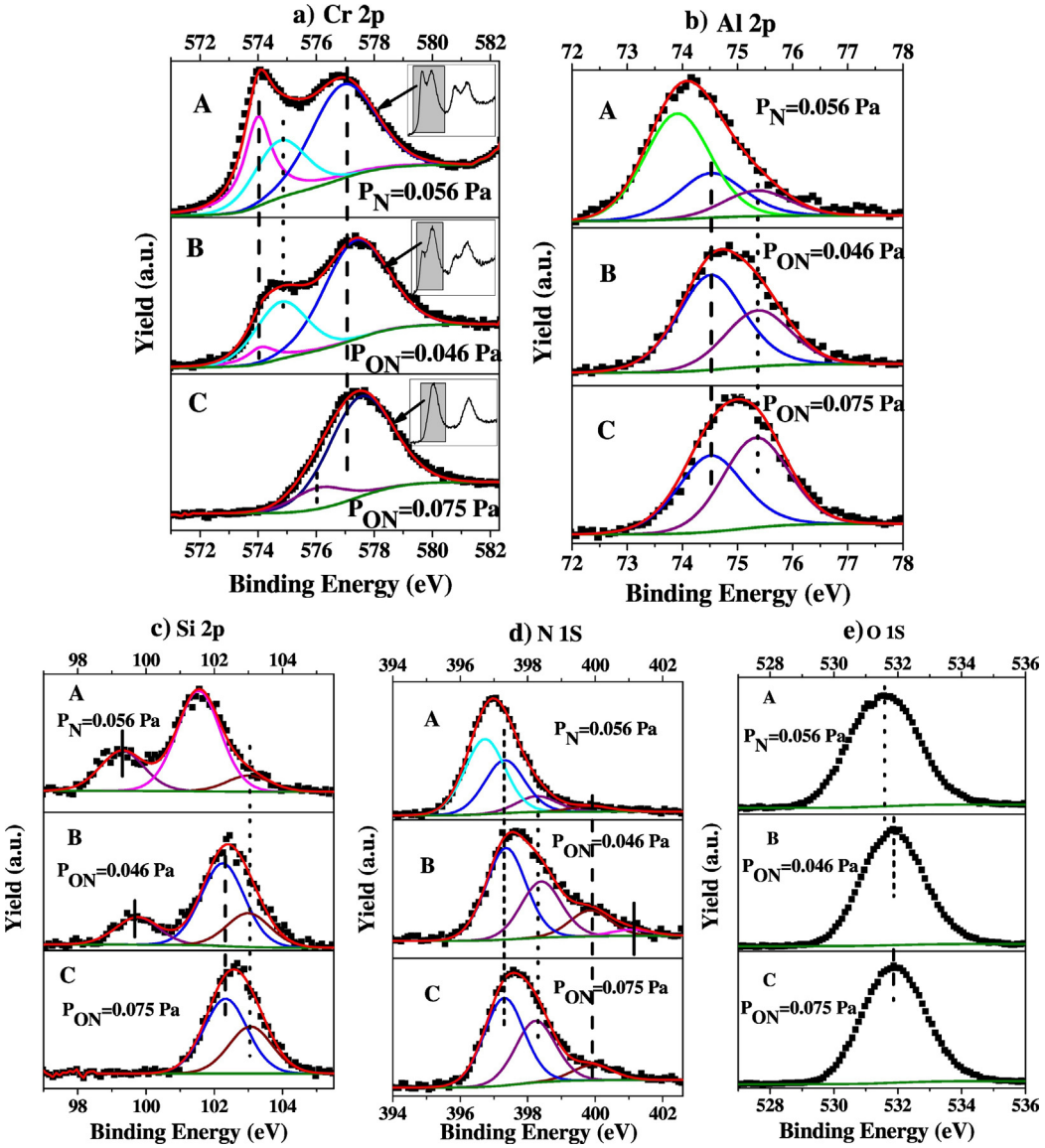

Fig. 5. XPS spectra of: (a) Cr 2p3/2, (b) Al 2p, (c) Si 2p, (d) N 1s and (e) O 1s electrons for the three samples: A, B and C. The green curve represents the background correction. (For interpretation of the references to colour in this figure legend, the reader is referred to the web version of this article.)

Table 3
Casa software fitting parameters and identification of core level binding energies.

Core peak	FWHM (eV)	BE(eV) sample A	BE(eV) sample B	BE(eV) sample C	Compound
Cr2 p3/2	1.2	574	574.1	–	Cr-Cr
	2.6	574.8	574.8	–	Cr-N
	2.1	576.9	577.4	577.5	Cr-O; Cr-$(OH)_3$
	2.1	–	–	576.1	Cr-O; Cr_2N
Al 2p	1.4	73.9	–	–	Al-N
	1.4	74.5	74.5	74.5	Al-(OH)
	1.4	75.4	75.4	75.3	Al-O
Si 1 s	1.5	99.3	99.7		*Si*-Si(Al)
	1.5	101.5	–		Si_3N_4
	1.5	–	102.3	102.3	Si(Al)-Si_2O_2; Si(Al)-SiO_2N
	1.5	103.0	103.0	103.0	Si(Al)-SiO_3; Si-O_4
N 1 s	1.4	396.7	–	–	Al-N
	1.4	397.3	397.4	397.3	Si_3N_4
	1.4	398.3	398.4	398.2	chromium oxynitride
	1.4	399.9	399.9	399.9	N-(C = O); Si(Al)-O_2N_2
	1.4	–	401.1	–	CH = N-CH

XRD results revealed that the two samples $CrAlSiN_x$ with $P_N = 0.15$ Pa and $CrAlSiOyN_x$ with $P_{NO} = 0.21$ Pa are polycrystalline with cubic (fcc-B_1) structure, with CrN peaks (111), (200), (220) and (222) at expected position as shown in Fig. 6 [1,54]. Fig. 7 represents cross-sectional SEM micrographs of several films that show the structure and the thickness as varying reactive gases partial pressure.

The amorphous structure of the films is mainly due to the high amount of aluminum and silicon in the films, and due to the sub-stoichiometry of the films [(O + N) / (Cr + Al + Si) <1]. In oxynitride case, it can be due to the fact that the mobility of oxygen in the growth surface of amorphous films is not sufficient to form oxide lattice [1].

As all samples that measured by Raman spectroscopy were amorphous, it was found that the detection of their elemental vibrational modes is so difficult by using Raman spectroscopy with used incident power conditions (very low laser incidence power), as shown in Fig. 8 [52,55].

The Raman spectra of the $CrAlSiN_x$ films (not shown), although amorphous, show two broad bands at approximately 190 cm^{-1} and 250 cm^{-1}. According to the literature [56] the fcc structure of $Al_{70}Cr_{30}N$ presents Raman bands at 260 and 750 cm^{-1}, being the low wavenumber band the most intense one. Furthermore, the wurtzite

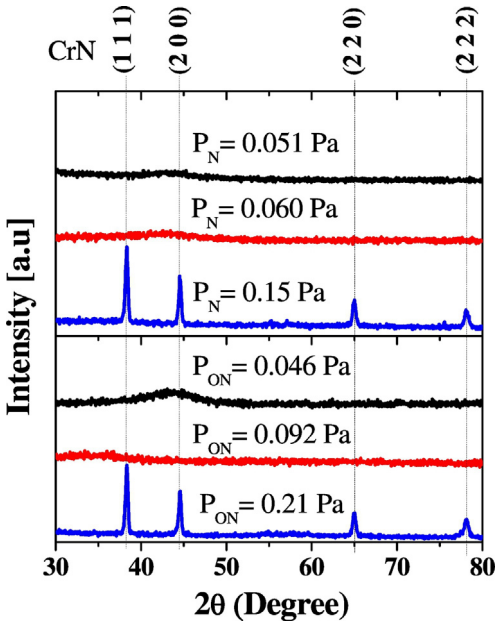

Fig. 6. XRD difractograms of $CrAlSiN_x$ and $CrAlSiO_y N_x$ films for different nitrogen and oxygen partial pressures.

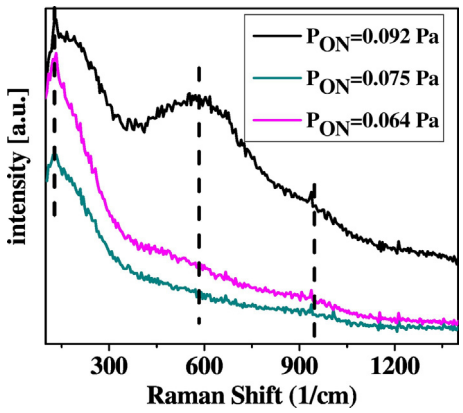

Fig. 8. Raman spectra of chosen CrAlSiON samples.

structure of $Al_{85}Cr_{15}$ N shows bands at 180 and 570 cm^{-1}, being the most intense the first one. In both cases the low frequency mode corresponds to vibrational acoustic modes (LA and TA) related with vibration of Cr ions and the high frequency one to vibrational optic modes (LO and TO) due to vibration of N ions [52,55]. According to our Raman spectra, we concluded that the $CrAlSiN_x$ shows a mixture of wurtzite + fcc-phases.

The peak position, FWHM and intensity of the bands were obtained by fitting the Raman spectra using Lorentzian functions. Interesting to note that the integrated intensity ratio between the 190 cm^{-1} mode (wurtzite) and 260 cm^{-1} mode (fcc structure is 2.4; 1.8 and 2 for respectively for $N_{P=0.051\ Pa}$, $N_{P=0.056\ Pa}$, $N_{P=0.060\ Pa}$ samples, indicating an increase of the fcc- structure as the nitrogen partial pressure increases.

On other hand, the intensity ratio between the 190 and 260 modes of $CrAlSiO_yN_x$ is lower than for the $CrAlSiN_x$ samples, ranging from 1.3 ($NO_{P=0.075\ Pa}$) to 1.8 ($NO_{P=0.046\ Pa}$). This low intensity ratio indicates that the presence of oxygen in the layer is not favourable to the formation of wurtzite structure.

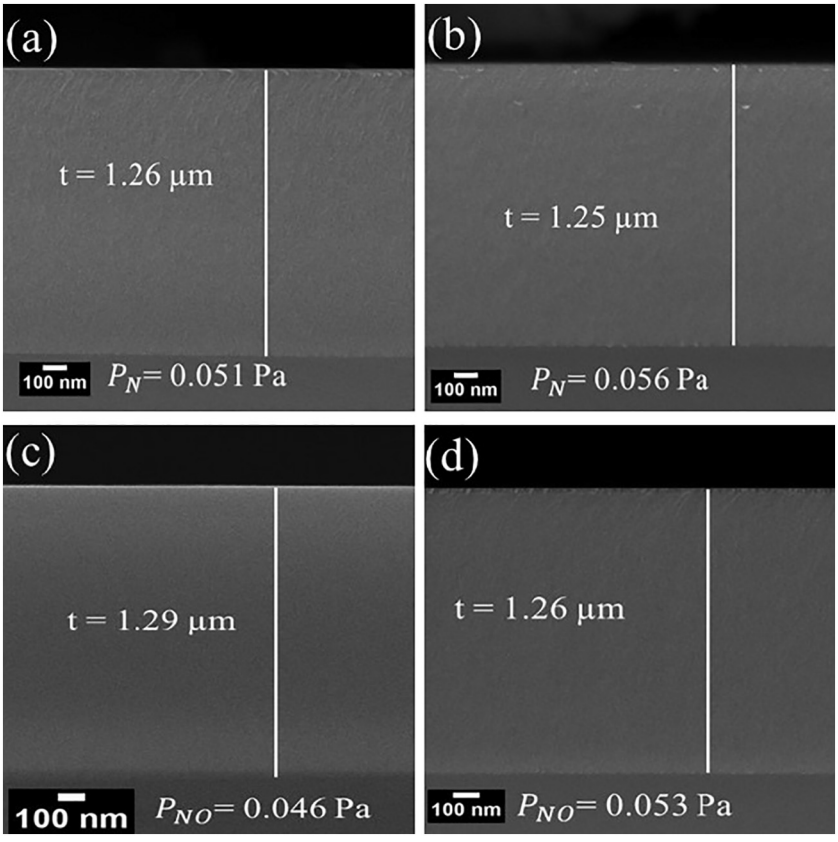

Fig. 7. Cross-sectional micrographs show the amorphous structure of (a) $CrAlSiN_x$ with nitrogen partial pressure 0.056 Pa and (b) $CrAlSiO_yN_x$ with nitrogen and oxygen partial pressure 0.053 Pa. In the figure, t means film thickness.

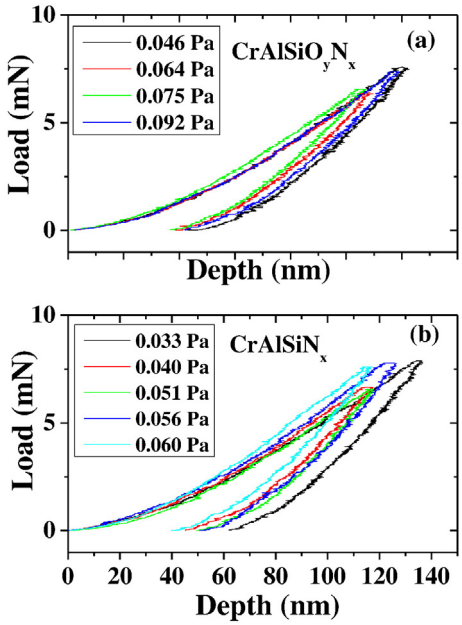

Fig. 9. Load – depth curves of (a) $CrAlSiO_yN_x$ as varying P_{ON} and (b) $CrAlSiN_x$ as varying P_N.

3.4. Mechanical properties

To probe the mechanical properties of the films, such as hardness and elastic modulus, a nanoindentation method has been applied to the thick samples deposited on polished stainless steel substrates. The maximum load was selected in order to have the indenter penetration depth lower than 10% of the coating thickness, and this is why the maximum load is below 8 mN, as shown in Fig. 9, where the load depth curves are represented for one measurement of each sample.

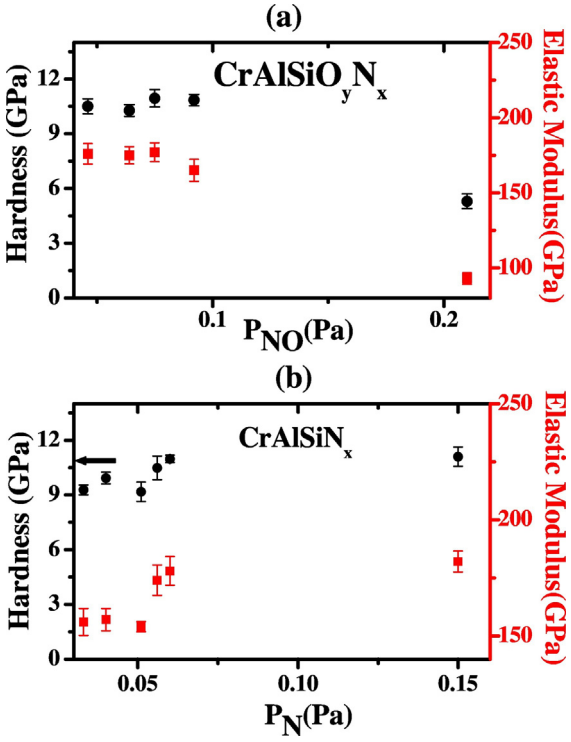

Fig. 10. Hardness and elastic modulus of (a) $CrAlSiO_yN_x$ as a function of P_{ON} and (b) $CrAlSiN_x$ as function of P_N.

The evaluation of hardness and elastic modulus with increasing P_N and P_{ON} are presented in Fig. 10. With increasing P_{ON} from 0.046 Pa to 0.92 Pa, no significant changes were seen in the hardness values (Fig. 10a). On the other hand, a notable decrement was seen in the hardness and elastic modulus values when P_{NO} increased to 0.21 Pa. This means that higher content of oxygen in films changes the structural bonds to weak metallic bonding. For nitrides films, hardness was slightly increased with increasing P_N from 0.051 Pa to 0.15 Pa. The highest obtained value was 11.1 GPa at 0.15 Pa, as shown in Fig. 10b. Hardness values are relatively low, but it is in the same range of magnitudes obtained by Karimi et al. [1] [8] with oxygen ratio [O] / [O + N] in films up to 20%. In those studies, the ratio (Al + Si) / Cr ~1 while in our case (Al + Si) / Cr ~2, which has a strong influence on the film properties. The substoichiometry and the amorphous phase fraction can be considered as other factors of poor hardness.

Depending on the results discussed in section 3, the variation of nitrogen and oxygen partial pressures induces an increase of those elements in sample composition, as expected. In addition to the strong variation of films' optical properties. However, the hardness is almost insensitive to the variation of those partial pressures, mainly due to the elemental Cr: Al: Si composition ratio of 1.25:1.5:1. The Optical constants of $CrAlSiN_x$ and $CrAlSiO_yN_x$ samples are very sensitive to nitrogen and oxygen partial pressures. The most appropriate ranges of P_N and P_{NO} for selective solar absorber stacks are 0.037–0.071 Pa and 0.046–0.092 Pa respectively.

4. Conclusions

Optical properties, chemical composition, chemical structure and mechanical properties of sputtered $CrAlSiN_x$ and $CrAlSiO_yN_x$ as varying P_N and P_{ON} have been studied in this work. Optical constants n and k decrease with increasing P_N and P_{ON}, and the refractive index increases in the wavelength range of 250–1000 nm for all coatings. According to chemical composition, the elemental composition ratio (Cr + Al + Si) / (N + O) decreases with increasing nitrogen and oxygen partial pressure. However, the elemental Cr: Al: Si composition ratio remains constant as 1.25: 1.5: 1. XPS data analysis shows that the at% of the sample changes with the variation of oxygen and nitrogen partial pressure, with nitrogen contact changing from 19.3 at% in nitride (sample A) to 10.1 at and 8.7 at% in oxynitrides (sample B and C, respectively). Additionally, XPS reveals an Al surface enrichment, because in the sample analyzed by XPS the (Al + Si) / Cr composition ratio is in average 2 times higher than that obtained by RBS and EDS, together with an increment of Al/Si composition ratio. Coatings with higher nitrogen and oxygen content are polycrystalline with cubic (fcc-B_1) structure. On contrary, all other films are amorphous and show poor hardness.

Acknowledgements

The authors acknowledge the support of FCT in the framework of the Strategic Funding UID/FIS/04650/2013 and the financial support of FCT, POCI and PORL operational programs through the project POCI-01-0145-FEDER-016907 (PTDC/CTM-ENE/2882/2014), co-financed by European community fund FEDER.

Appendix A. Supplementary data

Supplementary data to this article can be found online at http://dx.doi.org/10.1016/j.surfcoat.2017.08.038.

References

[1] H. Najafi, A. Karimi, M. Morstein, Correlation Between the Oxygen Content and the Structure of AlCrSiO x N (1-x) Thin Films Deposited by Pulsed DC Magnetron Sputtering Institute of Condensed Matter Physics (ICMP), Ecole Polytechnique Fédérale de Lausanne (EPFL) 1 (2010) 631–634.

[2] H. Chen, Y. Chan, J. Lee, J. Duh, Surface & Coatings Technology Oxidation Behavior of Si-Doped Nanocomposite CrAlSiN Coatings, 205, 2010 1189–1194, http://dx.doi.org/10.1016/j.surfcoat.2010.08.156.

[3] L. Castaldi, D. Kurapov, A. Reiter, V. Shklover, P. Schwaller, J. Patscheider, High temperature phase changes and oxidation behavior of Cr-Si-N coatings, Surf. Coat. Technol. 202 (2007) 781–785, http://dx.doi.org/10.1016/j.surfcoat.2007.05.070.

[4] L. Castaldi, D. Kurapov, A. Reiter, V. Shklover, P. Schwaller, J. Patscheider, Effect of the oxygen content on the structure, morphology and oxidation resistance of Cr-O-N coatings, Surf. Coat. Technol. 203 (2008) 545–549, http://dx.doi.org/10.1016/j.surfcoat.2008.05.018.

[5] M. Hirai, H. Saito, T. Suzuki, H. Suematsu, W. Jiang, K. Yatsui, Oxidation behavior of Cr-Al-N-O thin films prepared by pulsed laser deposition, Thin Solid Films 407 (2002) 122–125, http://dx.doi.org/10.1016/S0040-6090(02)00024-X.

[6] T.D. Nguyen, S.K. Kim, D.B. Lee, High-temperature oxidation of nano-multilayered TiAlCrSiN thin films in air, Surf. Coat. Technol. 204 (2009) 697–704, http://dx.doi.org/10.1016/j.surfcoat.2009.09.008.

[7] D.B. Lee, T.D. Nguyen, S.K. Kim, Air-oxidation of nano-multilayered CrAlSiN thin films between 800 and 1000 C, Surf. Coat. Technol. 203 (2009) 1199–1204, http://dx.doi.org/10.1016/j.surfcoat.2008.10.011.

[8] A. Karimi, M. Morstein, T. Cselle, Influence of oxygen content on structure and properties of multi-element AlCrSiON oxynitride thin films, Surf. Coat. Technol. 204 (2010) 2716–2722, http://dx.doi.org/10.1016/j.surfcoat.2010.02.029.

[9] Y. Chang, W. Chiu, J. Hung, Mechanical properties and high temperature oxidation of CrAlSiN/TiVN hard coatings synthesized by cathodic arc evaporation, Surf. Coat. Technol. 303 (2016) 18–24, http://dx.doi.org/10.1016/j.surfcoat.2016.02.047.

[10] Q.M. Wang, A superhard CrAlSiN superlattice coating deposited by a multi-arc ion plating: II. Thermal stability and oxidation, Surf. Coat. Technol. 214 (2015) 153–159, http://dx.doi.org/10.1016/j.surfcoat.2012.05.143.

[11] C. Hsu, D. Chen, A study on the abrasive and erosive wear behavior of arc-deposited Cr-N-O coatings on tool steel, Thin Solid Films 517 (2009) 1655–1661, http://dx.doi.org/10.1016/j.tsf.2008.09.083.

[12] R. Fors, Mechanical Properties and Thermal Stability of Reactive arc Evaporated Ti-Cr-al-N Coatings Rikard Forsén, 2012.

[13] X. Pang, K. Gao, F. Luo, H. Yang, L. Qiao, Y. Wang, A.A. Volinsky, Annealing effects on microstructure and mechanical properties of chromium oxide coatings, Thin Solid Films 516 (2008) 4685–4689, http://dx.doi.org/10.1016/j.tsf.2007.08.083.

[14] T. Polcar, A. Cavaleiro, High-temperature tribological properties of CrAlN, CrAlSiN and AlCrSiN coatings, Surf. Coat. Technol. 206 (2011) 1244–1251, http://dx.doi.org/10.1016/j.surfcoat.2011.08.037.

[15] T. Polcar, T. Vitu, J. Sondor, A. Cavaleiro, Tribological performance of CrAlSiN coatings at high temperatures, Plasma Process. Polym. 6 (2009)http://dx.doi.org/10.1002/ppap.200932307.

[16] Q.M. Wang, Y.N. Wu, M.H. Guo, P.L. Ke, J. Gong, C. Sun, L.S. Wen, Ion-plated Al-O-N and Cr-O-N films on Ni-base superalloys as diffusion barriers, Plasma Process. Polym. 197 (2005) 68–76, http://dx.doi.org/10.1016/j.surfcoat.2004.09.022.

[17] W. Ho, C.H. Shen, C.L. Chang, D.Y. Wang, Corrosion behaviors of Cr(N,O)/CrN multilayered coatings by cathodic arc deposition, Plasma Process. Polym. 202 (2007) 745–749, http://dx.doi.org/10.1016/j.surfcoat.2007.07.113.

[18] W. Ho, C.H. Shen, C.L. Chang, D.Y. Wang, Characteristics of PVD-CrAlSiN Films After Post-Coat Heat Treatments in Nitrogen Atmosphere, 2014http://dx.doi.org/10.1016/j.apsusc.2010.11.137.

[19] Y. Qiu, S. Zhang, J. Lee, B. Li, Y. Wang, D. Zhao, D. Sun, Towards Hard yet Self-Lubricious CrAlSiN Coatings, 618, 2015 132–138, http://dx.doi.org/10.1016/j.jallcom.2014.08.132.

[20] J.D. Lee, Q.M. Wang, S.H. Kim, T.G. Wang, D.W. Shin, K.H. Kim, Microstructure and mechanical properties of quaternary Cr-Si-O-N films by a hybrid coating system, Surf. Coat. Technol. 206 (2012) 3721–3727, http://dx.doi.org/10.1016/j.surfcoat.2011.11.012.

[21] V. Chawla, D. Puri, S. Prakash, B. Sidhu, Salt fog corrosion behavior of nanostructured TiAlN and AlCrN hard coatings on ASTM-SA213-T-22 boiler steel, Jordan J. Mech. Indust. Eng. 5 (2011) 247–253, http://dx.doi.org/10.4236/jmmce.2010.911075.

[22] S.K. Tien, C.H. Lin, Y.Z. Tsai, J.G. Duh, Effect of nitrogen flow on the properties of quaternary CrAlSiN coatings at elevated temperatures, Surf. Coat. Technol. 202 (2007) 735–739, http://dx.doi.org/10.1016/j.surfcoat.2007.06.042.

[23] C. Zou, W. Xie, L. Shao, Functional multi-layer solar spectral selective absorbing coatings of AlCrSiN/AlCrSiON/AlCrO for high temperature applications, Sol. Energy Mater. Sol. Cells 153 (2016) 9–17, http://dx.doi.org/10.1016/j.solmat.2016.04.007.

[24] C. Lampert, Microstructure of a black chrome solar selective absorber, in: SPIE 22nd International Technical Symposium, San Diego, n.d.

[25] W. Zhou, Y. Shen, E. Hu, Y. Zhao, M. Sheng, Y. Zheng, S. Wang, Y. Lee, C. Wang, D.W. Lynch, L. Chen, Nano-Cr-film-based solar selective absorber with high photo-thermal conversion efficiency and good thermal stability, Opt. Express 20 (2012) 28953–28962, http://dx.doi.org/10.1364/OE.20.028953.

[26] A. Ambrosini, T.N. Lambert, M. Bencomo, A. Hall, K. VanEvery, N.P. Siegel, C.K. Ho, Improved high temperature solar absorbers for use in concentrating solar power central receiver applicationsASME 2011 5th Int. Conf. Energy Sustain 2011, pp. 587–594, http://dx.doi.org/10.1115/ES2011-54241.

[27] S. Khamlich, Black Cr/α-Cr2O3 nanoparticles based solar absorbers, Phys. B Phys. Condens. Matter. 407 (2011) 1509–1512, http://dx.doi.org/10.1016/j.physb.2011.09.073.

[28] A.B.C. EKWEALOR, Variations of optical and structural propertis with temperature for CrxOy thin films synthesizd in a polymer matrix by chemical bath deposition thechnique, Dig. J. Nanomater. Biostruct. 9 (2014) 423–431.

[29] P. Carcia, G. Hughes, R. French, C. Torardi, G. Reynolds, L. Dieu, Thin films for phase-shift masks, Vac. Thin Film, 1999.

[30] F.D. Lai, L.A. Wang, Fabrication and characterization of aluminum oxide/chromium oxide superlattice for attenuated phase-shifting mask working at 193 nm wavelength, Thin Solid Films 409 (2002) 220–226, http://dx.doi.org/10.1016/S0040-6090(02)00137-2.

[31] A. Inspektor, P.A. Salvador, Architecture of PVD coatings for metalcutting applications: a review, Surf. Coat. Technol. 257 (2014) 138–153, http://dx.doi.org/10.1016/j.surfcoat.2014.08.068.

[32] J.M. Wheeler, R. Raghavan, V. Chawla, M. Morstein, J. Michler, Deformation of hard coatings at elevated temperatures, Surf. Coat. Technol. 254 (2014) 382–387, http://dx.doi.org/10.1016/j.surfcoat.2014.06.048.

[33] A. Pélisson, M. Parlinska-Wojtan, H.J. Hug, J. Patscheider, Microstructure and mechanical properties of Al-Si-N transparent hard coatings deposited by magnetron sputtering, Surf. Coat. Technol. 202 (2007) 884–889, http://dx.doi.org/10.1016/j.surfcoat.2007.05.094.

[34] J.W. Kim, K.H. Kim, D.B. Lee, J.J. Moore, Study on high-temperature oxidation behaviors of Cr-Si-N films, Surf. Coat. Technol. 200 (2006) 6702–6705, http://dx.doi.org/10.1016/j.surfcoat.2005.10.004.

[35] S. Khamseh, M. Nose, T. Kawabata, A. Saiki, K. Matsuda, K. Terayama, S. Ikeno, Effect of deposition conditions on the structure and properties of CrAlN films prepared by pulsed DC reactive sputtering in FTS mode at high al content, Japan Inst. Met. 49 (2008) 2082–2090, http://dx.doi.org/10.2320/matertrans.MRA2008604.

[36] H. Najafi, A. Karimi, D. Alexander, P. Dessarzin, M. Morstein, Effects of Si and Y in structural development of (Al,Cr,Si/Y)OxN1−x thin films deposited by magnetron sputtering, Thin Solid Films 549 (2013) 224–231, http://dx.doi.org/10.1016/j.tsf.2013.06.062.

[37] C. Oliver, M. Pharr, An improved technique for determining hardness and elastic modulus using load and displacement sensing indentation experiments, J. Mater. Res. 7 (1992) 1564–1583, http://dx.doi.org/10.1557/JMR.1992.1564.

[38] N.P. Barradas, C. Jeynes, Advanced physics and algorithms in the IBA DataFurnace, Nucl. Instrum. Methods Phys. Res., Sect. B 266 (2008) 1875–1879, http://dx.doi.org/10.1016/j.nimb.2007.10.044.

[39] N. Fairely, CasaXPS Manual 2.3. 15, Casa Softw. Ltd., 2009 1–177http://scholar.google.com/scholar?hl=en&btnG=Search&q=intitle:CasaXPS+Manual+2.3.15#2.

[40] M. Fox, Optical Properties of Solids, Oxford University Press Inc., NewYork, 2001.

[41] W. Theiss, SCOUT Thin Film Analysis Software Handbook, 2002.

[42] Y.P. Purandare, A.P. Ehiasarian, P.E. Hovsepian, Sputtering and unbalanced magnetron sputtering technique Target poisoning during CrN deposition by mixed high power impulse magnetron sputtering and unbalanced magnetron sputtering technique, Am. Vac. Soc. 41502 (2016)http://dx.doi.org/10.1116/1.4950886.

[43] M. Hassel, I. Hemmerich, H. Kuhlenbeck, H. Freund, High resolution XPS study of a thin Cr2O3(111) film grown on Cr(110), Surf. Sci. Spectra. 4 (1998) 246–252, http://dx.doi.org/10.1116/1.1247795.

[44] M.C. Biesinger, B.P. Payne, A.P. Grosvenor, L.W.M. Lau, A.R. Gerson, R.S.C. Smart, Resolving surface chemical states in XPS analysis of first row transition metals, oxides and hydroxides: Cr, Mn, Fe, Co and Ni, Appl. Surf. Sci. 257 (2011) 2717–2730, http://dx.doi.org/10.1016/j.apsusc.2010.10.051.

[45] A. Conde, A.B. Cristóbal, G. Fuentes, T. Tate, J. de Damborenea, Surface analysis of electrochemically stripped CrN coatings, Surf. Coat. Technol. 201 (2006) 3588–3595, http://dx.doi.org/10.1016/j.surfcoat.2006.08.110.

[46] B. Subramanian, M. Jayachandran, Preparation of chromium oxynitride and chromium nitride films by DC reactive magnetron sputtering and their material properties, Corros. Eng. Sci. Technol. 46 (2011) 554–561, http://dx.doi.org/10.1179/147842209X12579401586807.

[47] W. Zhao, F.J. DiSalvo, Direct access to macroporous chromium nitride and chromium titanium nitride with inverse opal structure, Chem. Commun. 51 (2015) 4876–4879, http://dx.doi.org/10.1039/C4CC09564B.

[48] L. Rebouta, A. Sousa, M. Andritschky, F. Cerqueira, C.J. Tavares, P. Santilli, K. Pischow, Solar selective absorbing coatings based on AlSiN/AlSiON/AlSiOy layers, Appl. Surf. Sci. 356 (2015) 203–212, http://dx.doi.org/10.1016/j.apsusc.2015.07.193.

[49] W. Österle, I. Dörfel, I. Urban, T. Reier, J.W. Schultze, XPS and XTEM study of AlN formation by N+2 implantation of aluminium, Surf. Coat. Technol. 102 (1998) 168–174, http://dx.doi.org/10.1016/S0257-8972(98)00355-7.

[50] S. Ladas, L. Sygellou, S. Kennou, M. Wolf, G. Roeder, A. Nutsch, M. Rambach, W. Lerch, An X-ray photoelectron spectroscopy study of ultra-thin oxynitride films, Thin Solid Films 520 (2011) 871–875, http://dx.doi.org/10.1016/j.tsf.2011.04.161.

[51] P. Cova, S. Poulin, O. Grenier, R.A. Masut, A method for the analysis of multiphase bonding structures in amorphous SiOxNy films, J. Appl. Phys. 97 (2005)http://dx.doi.org/10.1063/1.1881774.

[52] H.C. Barshilia, N. Selvakumar, B. Deepthi, K.S. Rajam, A comparative study of reactive direct current magnetron sputtered CrAlN and CrN coatings, Surf. Coat. Technol. 201 (2006) 2193–2201, http://dx.doi.org/10.1016/j.surfcoat.2006.03.037.

[53] R.T. Haasch, Epitaxial ScN(001) grown and analyzed in situ by XPS and UPS. II. Analysis of Ar+ sputter etched layers, Surf. Sci. Spectra. 7 (2000) 178, http://dx.doi.org/10.1116/1.1365377.

[54] M. Stüber, U. Albers, H. Leiste, K. Seemann, C. Ziebert, S. Ulrich, Magnetron sputtering of hard Cr-Al-N-O thin films, Surf. Coat. Technol. 203 (2008) 661–665, http://dx.doi.org/10.1016/j.surfcoat.2008.04.083.

[55] R. Kaindl, B. Sartory, J. Neidhardt, R. Franz, A. Reiter, P. Polcik, R. Tessadri, C. Mitterer, Semi-quantitative chemical analysis of hard coatings by Raman micro-spectroscopy: the aluminium chromium nitride system as an example, Anal. Bioanal. Chem. 389 (2007) 1569–1576, http://dx.doi.org/10.1007/s00216-007-1540-4.

[56] J. Soldán, J. Neidhardt, B. Sartory, R. Kaindl, R.Č.P.H. Mayrhofer, Structure – property relations of arc-evaporated Al – Cr – Si – N coatings, Surf. Coat. Technol. 202 (2008) 3555–3562, http://dx.doi.org/10.1016/j.surfcoat.2007.12.041.